# Hydration Force between Mica Surfaces in Aqueous KCl Electrolyte Solution

**ARTICLE** *in* LANGMUIR · FEBRUARY 2012

Impact Factor: 4.46 · DOI: 10.1021/la204603y · Source: PubMed



**1 AUTHOR:**

Yongsheng Leng
George Washington University
**56** PUBLICATIONS **767** CITATIONS

Langmuir

Article

pubs.acs.org/Langmuir

# Hydration Force between Mica Surfaces in Aqueous KCl Electrolyte Solution

Yongsheng Leng*

Department of Mechanical and Aerospace Engineering, The George Washington University, Washington, DC 20052, United States

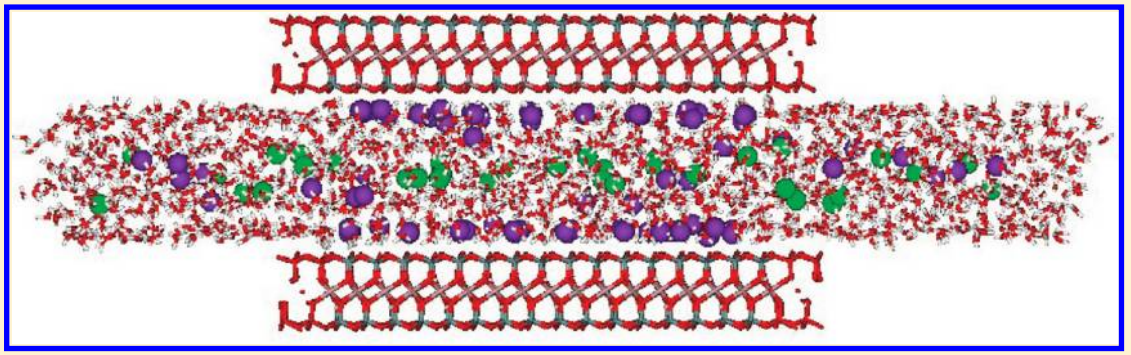

**ABSTRACT:** Liquid−vapor molecular dynamics simulations are performed to study the interaction forces between two mica surfaces in an aqueous KCl electrolyte solution. Strong repulsive hydration force is obtained within a distance of ∼2 nm between the two mica surfaces, which cannot be explained by the continuum theory of double-layer repulsion. We find that this short-range repulsive hydration force is much stronger than the double-layer force between mica surfaces. Whereas the simulation system is much smaller than the surface force measurement system, fundamental mechanisms of repulsive hydration force are revealed. In particular, important features of the step-like force oscillatory behavior during normal compression and force hysteresis during retraction are observed. Detailed analysis of the ionic density distributions shows that the "forced adsorption" of diffusive $K^+$ ions onto mica surfaces during compression and the subsequent "slow desorption" of the absorbed $K^+$ ions from mica surfaces upon retraction are responsible for the hysteresis phenomenon. From a mechanics point of view, we attribute the load bearing capacity of the dense electrolyte to the very hard hydration shells of $K^+$ metal ions under confinement. We find that the hydrated $K^+$ ions and $Cl^-$ co-ions remain very diffusive in the aqueous film. Water molecules in the hydration layer are also very fluidic, in the sense that the diffusion constant of water molecules is less than its bulk value by at most 3 orders of magnitude under the extreme confinement.

## I. INTRODUCTION

The mechanism of repulsive hydration force between two charged solid surfaces in electrolyte salt solutions has been studied extensively for decades.[1−13] The broad interests to this topic originate from its wide applications in many fields, such as hydration forces between lipid membranes and between macromolecules in cell biology,[14−16] colloidal interactions,[1,14] clay swelling and geochemical processes in geology,[17−19] biolubrication,[20−22] nanofluidics, and nanotribology.[23,24] Exploration of the fundamental questions in these fields has also resulted in substantial molecular simulation studies on the structure and dynamics of water molecules and ions in aqueous systems under confinements. These include hydration behavior of water confined between hydrophilic and hydrophobic surfaces,[25,26] water and ions in silica slit pores[27] and carbon nanotubes,[28,29] and between charged clay surfaces[30−36] and zwitterionic surfaces.[37] The mica−water contact has been widely used as a typical model system in surface force apparatus (SFA) experiments due to the ease of preparation of molecularly smooth mica surfaces. In particular, hydration structures of water and ion distributions at the mica−water interface have been investigated by different experimental techniques.[38−41] Recent studies by three-dimensional scanning force microscopy[41] directly revealed the very detailed adsorption structure of water near mica surfaces, which is consistent with the findings from the X-ray reflectivity measurements[39] and molecular simulations.[32−34,42] While the hydration structure at the mica−water interface has been investigated extensively in both experiments and molecular simulations, it would be more interesting to theoretically study how these structures and associated forces between two mica surfaces evolve during normal approach and retraction in an electrolyte salt solution.

Over 30 years ago, Israelachvili and Adam,[2] and later Pashley,[3,4] performed very detailed surface force measurements between two mica sheets in aqueous electrolyte solutions. In dilute electrolytes or acid solutions, the variation of the surface force versus mica gap distance follows the Derjaguin−Landau−Verwey−Overbeek (DLVO) theoretical prediction,[43,44] which states that the mutual repulsion between two mica surfaces at a

**Received:** November 22, 2011
**Revised:** February 20, 2012
**Published:** February 27, 2012





dx.doi.org/10.1021/la204603y | *Langmuir* 2012, 28, 5339−5349

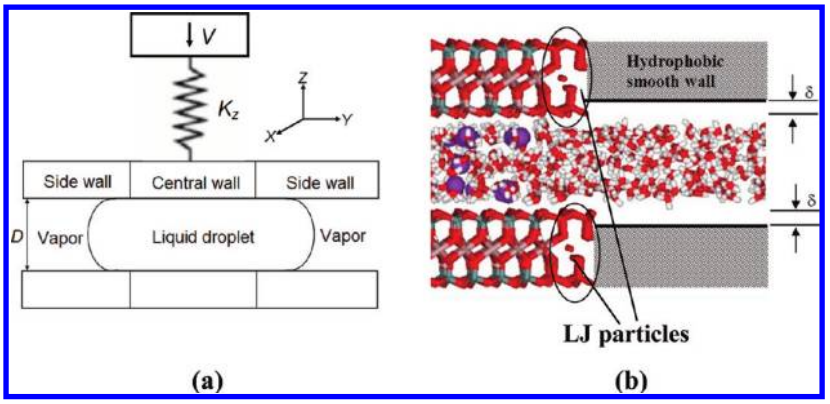


**Figure 1.** (a) Sketch of the liquid–vapor molecular dynamics (LVMD) model. (b) Local arrangements of mica surfaces, mica edge LJ particles, and hydrophobic smooth walls.

large distance and attractive collapse at a distance of a few nanometers are associated with the force balance between the electrostatic repulsive double-layer force and van der Waals attractive force. In very dense electrolytes, however, an additional strong repulsive force at short distances (particularly, in a distance less than a few nanometers), hydration force,[3] prevents van der Waals attractive collapse between two mica surfaces. Widely existing in nature, this short-range repulsive force is also responsible for the repulsion between two lipid bilayers in high-concentration salt solutions.[15] Clearly, the short-range hydration force is closely related to the role of hydrated metal ions and co-ions in the nanoconfined aqueous film.[8]

In their seminal work, Israelachvili and Pashley[5,7] further revealed that the repulsive force is not purely monotonic, but has an oscillatory component superimposed on it with the periodicity of the diameter of water molecules. The step-like feature of hydration force within a distance of ~1.5 nm indicated that water was squeezed out layer-by-layer in sequence. However, explanations to the physics of this hydration force are still quite controversial.[14,15] It has been claimed that either the anomalous dielectric response of water near charged surfaces,[45] or the effect of dielectric overscreening in electrostatics for water,[46] was responsible for the short-range repulsion. This is in contrast to the argument that water should not have a different dielectric constant near or between two surfaces.[14]

Because the force between two mica surfaces is one of the key elements being measured in the SFA experiment, direct simulation of the force measurement procedure through a proper molecular simulation approach will provide many insights into the hydration force mechanism. In a previous publication,[47] the hydration force between two mica surfaces in water was studied. In that work, a liquid–vapor molecular dynamics (LVMD) method was developed, in which a liquid droplet with two liquid–vapor interfaces was confined between two mica surfaces. Under compression, the coexistence of liquid and vapor phases (see panel a in Figure 1) allows the droplet to be freely squeezed out. This method prevents molecular trajectories from being disrupted due to the scaling of particle coordinates to control the pressure, while at the same time the lateral pressure is maintained negligibly low that is comparable to the ambient condition. Using the LVMD simulation method, we recently studied the liquid-to-solid phase transition of a simple nonpolar fluid under confinement[48] and its stick–slip friction.[49] The force profile obtained from simulation is remarkably similar to those in the surface force balance experiment.[50,51] To further validate the simulation method, we recently performed the grand-canonical Monte Carlo (GCMC) simulation to study the solvation force oscillation and phase transition of the same molecular system.[52] The similar results from the two simulation methods suggest that LVMD is a suitable tool to study the structure and dynamics of nanometer confined fluids in the SFA experiments.

The present study will focus on the molecular simulation of hydration force between two mica surfaces in a dense electrolyte, especially the origin of this repulsive force as two mica surfaces approach each other in a KCl electrolyte.[1,2,7] While the compression of the aqueous electrolyte by mica would involve dynamic changes of the associated hydration structures (water structure effects[14]), we find that the very rigid hydration shells of hydrated metal $K^+$ ions under confinement are largely responsible for the load bearing capacity of the dense electrolyte.

## II. MODEL AND SIMULATION METHOD

Figure 1 shows a schematic of the mechanical model in LVMD simulation. The upper confining wall is connected to a driving block through a spring to mimic the force measurement system. The central wall is a one-layer mica crystal connected to two smooth hydrophobic walls. An electrolyte droplet is introduced between two confining walls. The liquid–vapor interface is located in the hydrophobic pore with a distance away from the mica edges. The force between two surfaces in electrolyte is calculated on the basis of the central mica configuration, and the side hydrophobic walls only apply unidirectional constraints to the squeezed-out electrolyte (see below). Therefore, the liquid–vapor boundary will have minimal effect on the hydration force calculation as the droplet is squeezed out substantially. However, the Laplace pressure developed within the droplet and its contribution to the normal force between mica surfaces need to be considered. This effect on the hydration force calculation will be discussed in section III.A.

During the squeezing of the confined liquid droplet, the upper confining wall is pushed downward by the driving spring. At any equilibrium distance, the upper mica wall is subjected to the spring force and the surface force from the molecular system, which is the summation of all of the interatomic forces on the central mica surface. The normal spring constant ($k_z$) is taken as 150 N/m, a typical value used in the surface force balance.[51] The upper mica wall is also movable in the lateral directions. Periodic boundary conditions are applied to the


dx.doi.org/10.1021/la204603y | Langmuir 2012, 28, 5339–5349

three dimensions. A sufficiently large vacuum space above the upper confining wall is maintained in the simulation box to reduce the imaging force in the normal direction.

In the previous work,[47] attractive forces between the two mica surfaces at larger distances were found. While electrostatic interactions in a neutral system favor attractions between the two charged surfaces,[1] the unscreened charges associated with the mica edge atoms (such as surface O, tetrahedral Si, and octahedral Al in mica) also have strong attractions to water molecules and ions. To eliminate this effect, nonpolar Lennard-Jones (LJ) particles are introduced between the mica edge and the hydrophobic smooth wall to prevent direct contact between water molecules and mica edge atoms. The hydrophobic smooth walls are also shifted backward by a small distance $\delta \approx 1$ Å (see Figure 1) to enable the aqueous film to have a uniform thickness in the entire region (in both mica and hydrophobic pores).[53] The simulation box length in the $y$-direction (Figure 1) is sufficiently large to maintain a stable liquid−vapor interface.

A 1 M KCl electrolyte droplet is introduced between two mica surfaces at a distance of $D$ = 2.13 nm. The droplet contains 1655 TIP4P[54] water molecules, 34 $K^+$ ions, and 34 $Cl^-$ co-ions. The mica surface is a one-layer mica crystal with the clay mineral structure of 2:1 layered dioctahedral (hydroxyl-) aluminosilicate. In the present study, each mica surface consists of 4 × 4 unit cells with the muscovite formula $K_2Al_4(Al,Si_3)_2O_{20}(OH)_4$. One mica layer consists of one octahedral aluminum sheet sandwiched by two tetrahedral silicon sheets. Because of the substitution of Si by Al in the inner tetrahedral sheet with a ratio of Al:Si = 1:3, each mica surface has 32 additional $K^+$ ions to balance the charged sites. Interactions between water molecules and mica clay surfaces are described by the TIP4P water-rigid mica model,[31] which has been shown very successful to predict the clay swelling behaviors and especially the hydration structure of water near mica surface.[33,34] Water and ions ($K^+$ and $Cl^-$) interactions are described by the Bounds potential.[55] The LJ parameters for halide $Cl^-$ anions and alkali metal $K^+$ ions are obtained from recent optimized fittings.[56] All of these force parameters are summarized in Table 1.

In the hydrophobic pores, water molecules, $K^+$ ions, and $Cl^-$ co-ions are subject to unidirectional constraints by a 9-3 LJ surface potential[57] along the normal $z$-direction by the hydrophobic walls, and no reverse forces are applied to the walls. Consequently, the hydrophobic attractive force between two hydrophobic walls in aqueous solution[58] will not exist in the present study.

The unified expression for the atomic interactions between different species "$i$" and "$j$" (including O and H in TIP4P water, $K^+$ ion, and $Cl^-$ co-ion, and different atoms in mica crystals) in aqueous electrolyte can be written as:

$$u_{ij}(r) = \sum_{ij} (q_i q_j / r_{ij} + A_{ij}\exp(-B_{ij}r) - C_{ij}/r^4 - D_{ij}/r_{ij}^6 + E_{ij}/r_{ij}^{12}) \quad (1)$$

where $q_i$ is the electronic partial charge of particle $i$, and $A$, $B$, $C$, $D$, and $E$ are force constants. The detailed force field parameters are summarized in Table 1.

**Table 1. Force Field Parameters Used in Molecular Simulations**

| site | $q$ (e) | site | $q$ (e) | site | $q$ (e) |
|---|---|---|---|---|---|
| M ($H_2O$)[a] | −1.04[b] | O (apical) | −1.0[c] | Al (tetr) | 0.2[c] |
| H ($H_2O$, OH) | 0.52[b,c] | K | 1.0 | Al (oct) | 3.0[c] |
| O (surface) | −0.8[c] | Cl | −1.0 | $O_{edge}$ | 0.0 |
| O (OH) | −1.52[c] | Si | 1.2[c] | | |

| sites | $A$ (kcal/mol) | $B$ (Å$^{-1}$) | $C$ (kcal Å$^4$/mol) | $D$ (kcal Å$^6$/mol) | $E$ (kcal Å$^{12}$/mol) |
|---|---|---|---|---|---|
| O−O[b] | | | | 610.0 | 600 000.0 |
| O−K[d] | 53 884.0 | 3.339 | 438.0 | −638.0 | |
| H−K[d] | 5747.0 | 3.4128 | | | |
| Si−K[c] | 19.0 | 0.749 | | | |
| Al−K[c] | 19.0 | 0.749 | | | |
| Cl−O[d] | 8025.0 | 2.151 | 361.0 | | |
| $O_{edge}$−O[e] | | | | 610.0 | 600 000.0 |
| K−K[f] | | | | 38.2 | 729 317.3 |
| Cl−Cl[f] | | | | 11 986.0 | 50 586 074.2 |
| K−Cl[f] | | | | 676.66 | 6 073 985.4 |
| $O_{edge}$−K[e] | | | | 38.2 | 729 317.3 |
| $O_{edge}$−Cl[e] | | | | 38.2 | 729 317.3 |

[a]Massless site in TIP4P water molecule. [b]Reference 54. [c]Reference 31. [d]Reference 55. [e]Adjusted in this work. [f]Reference 56.

The dispersive interaction between Cl and H sites is described by a Morse potential:[55]

$$u_{Cl-H}(r) = D_{Cl-H}\{\exp[-\alpha(r - r_e)]\}\{\exp[-\alpha(r - r_e)] - 2\} \quad (2)$$

where $D_{Cl-H}$ = 1.2 kcal/mol, $\alpha$ = 2.80 Å$^{-1}$, and $r_e$ = 2.22 Å.

The SETTLE constraint dynamics algorithm[59] is used to propagate the trajectories of the TIP4P rigid water molecules with a time step of 2 fs. The long-range electrostatic interactions in the molecular system are calculated from the Ewald summation with a boundary correction term[60] for the slab geometry, and the cutoff for LJ interactions between different particles is 9 Å, as implemented in the TIP4P rigid mica model.[31] The temperature of the molecular system is controlled at 298 K by the external thermostat.[61]

## III. RESULTS AND ANALYSIS

**A. Hydration Force Simulation.** The procedure of LVMD simulation for the hydration force measurement is described below. Initially, after the molecular system is equilibrated at a mica gap distance of $D$ = 2.13 nm, the driving block begins to move downward with a driving velocity at 1 m/s. For the present molecular system, this driving velocity is below the critical value above which the hydrodynamic effect will be significant.[47] At every incremental driving distance of 1.5 Å, the molecular system will be allowed to equilibrate through a sufficiently long MD relaxation. At the beginning of relaxation, the driving spring is under compression, and the decaying of the spring force during relaxation is then monitored. When the spring force completely levels off, the system is considered to reach an equilibrium state. The hydration force is then calculated by averaging the spring forces over the last 1 ns MD equilibrium run. The variation of the averaged quasistatic spring force versus the thickness of aqueous film will give a typical force−distance profile, which is usually obtained in surface force measurements.


dx.doi.org/10.1021/la204603y | Langmuir 2012, 28, 5339−5349

*Force Profile during Normal Compression (Inward Approach).* Figure 2 shows the fluctuations of the normal

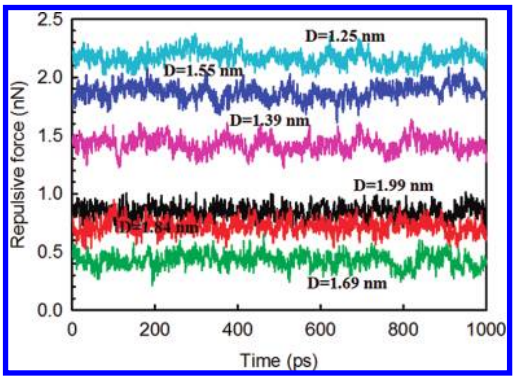


**Figure 2.** The fluctuations of repulsive normal forces of different hydration layers in the last 1 ns of MD equilibrium runs.

spring forces at different mica gap distances in the last 1 ns of MD equilibrium runs. For the thick electrolyte layers $D > 1$ nm, the time for the molecular system to reach equilibrium or the normal spring force to level off is usually less than 1 ns. However, for very thin layers, very long MD relaxations beyond many nanoseconds are needed. In the extreme case of $D = 0.75$ nm, which corresponds to two hydration layers, a 20 ns MD relaxation run is performed to calculate the static hydration force.

From the data shown in Figure 2, the force profile during normal compression versus the distance between two mica surfaces is drawn in Figure 3. Repulsive force is seen in the

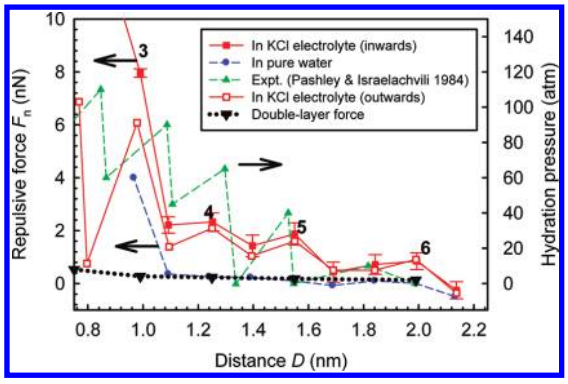


**Figure 3.** Repulsive hydration force profile between two mica surfaces in 1 M KCl electrolyte solution. The numerical numbers 6, 5, 4, and 3 represent different layers of hydration film. Experimental hydration pressures (green ▲, in the unit of MPa on the right axis) and continuum double-layer forces (▼) are also shown for comparison. Error bars indicate the force variance.

range of $D = 0.75-1.99$ nm, where the force magnitude in the range of 0−10 nN is shown in the figure. The force increases sharply when $D < 1.0$ nm. Because there are two liquid−vapor interfaces existing at the ends of the electrolyte droplet, which means that the lateral pressure should be comparable to the ambient pressure, the large repulsive forces observed in the normal direction suggest that the mechanical property of the confined electrolyte film is highly heterogeneous. Moreover, Figure 3 shows that the repulsive force is not monotonic, but has a step-like oscillatory feature in the range of $D = 1.09-2.13$ nm. The exponential decay length is estimated around 0.28 nm, close to the Debye length of the double layer force in 1 M KCl electrolyte (see the discussion in section III.D), as well as the diameter of water molecules. This force oscillatory behavior is very similar to what was observed in the SFA experiment by Pashley and Israelachvili.[7] However, more force oscillations were found in the experiment (the green line) due to the mica−glue deformation in SFA, which was clearly different from the present situation in the LVMD simulation.

To verify that the strong repulsive hydration force is indeed related to the hydrated $K^+$ ions and $Cl^-$ co-ions in the dense electrolyte, we recalculated the forces between the two mica surfaces in pure water, by simply removing the 34 $K^+$ ions and 34 $Cl^-$ co-ions in the aqueous film. In this case, as shown in Figure 3, the overall magnitude of the force between two mica surfaces in pure water (the blue line) is much smaller than those in 1 M KCl electrolyte. The strong repulsive force at $D <$ 1 nm in pure water is simply because of the overlaps of the adsorbed $K^+$ hydration shells near mica surfaces.[47,62]

*Contribution of Meniscus Force to the Hydration Force.* It is worth noting that in LVMD simulations, the existence of two liquid−vapor interfaces in the hydrophobic zone will introduce an extra meniscus force, which is contributed from the Laplace pressure and circumferential surface tension.[1,63,64] As has been discussed in section II, the surface tension occurs in the hydrophobic zone far from the central mica surface. Therefore, it would not contribute toward the hydration force. However, the Laplace pressure will have a contribution instead, which is equal to the integration of this pressure over the meniscus area. Because only the atomic interaction forces in the mica crystals are involved in accounting the hydration force, the meniscus area should be the mica contact area. For an aqueous droplet shown in Figure 1, the Laplace pressure could be estimated as:[1]

$$P_L = \gamma_L / r_y \tag{3}$$

where $\gamma_L$ is the surface tension of water, and $r_y$ is the radius of curvature in the $y$-direction. At nanometer scales, we find that the surface tension of water is comparable to its bulk value.[65] Assuming that $\gamma_L = 60$ mN/m, $r_y$ could be directly estimated from the convex-shaped menisci (see Figure 6 in section III.B). For the present simulation system, the contact area between the two central mica surfaces is $A = 4.15$ nm × 3.60 nm = 15 nm$^2$. Under the extreme confinement of $D = 0.75$ nm in which the Laplace pressure reaches the maximum, the repulsive force component contributed from the Laplace pressure could be as large as ~1.2 nN (assuming $r_y$ is comparable to the aqueous film thickness, $D = 0.75$ nm). This extra repulsive force component is roughly 1 order of magnitude smaller than the total repulsive force obtained from LVMD simulation (see Figure 3).

*Force Profile during Normal Separation (Outward Retraction).* Similar to the SFA experiment, retraction simulations are also performed to study adhesion hysteresis. Figure 3 shows the force profile starting at $D = 0.75$ nm outward, which corresponds to the two hydration layers. The simulated force−distance curve upon separation also shows a step-like oscillatory feature, but is below the inward force−distance curve. The results are similar to the force law observed in SFA experiment.[7] In particular, large hysteresis is observed at distance $D < 1$ nm. This hysteresis gradually disappears at $D =$ 1.55 nm, or at 5 hydration layers. Origin of this hysteresis will be discussed in section III.B. For comparison, we note that in our previous work on the normal approach and retraction between two crystals in a simple nonpolar fluid, significant


dx.doi.org/10.1021/la204603y | *Langmuir* 2012, 28, 5339−5349

adhesion hysteresis and large adhesion forces were observed during retraction, which was originated from the solid−liquid−solid phase transition.[48]

*Contact Mechanics Involved in SFA Experiment and LVMD Simulation.* We now consider the fundamental difference in contact mechanics between the SFA experiment and the present LVMD simulation. In SFA the contact between two cylindrically curved mica sheets[2] in cross contact is equivalent to the contact between an elastic sphere and a flat surface.[66] As the two mica surfaces are gradually pushed together in electrolyte, the hydration pressure developed in the confined aqueous film will flatten the mica substrate due to the very compliant visco-elastic behavior of the mica−glue complex on the glass substrate.[7] Assuming the hydration pressure is similar to the Hertz contact pressure, from the contact mechanics analysis[66] one can find that the relation between the mean pressure ($p_m$) in the contact area and the contact load ($F$) follows the "1/3" power law, that is, $p_m \approx F^{1/3}$. In the present LVMD simulation, however, the rigid mica surface and the constant contact area in the central mica pore will make the contact pressure directly proportional to the normal force, $F$. Consequently, for the same contact load, the LVMD simulation will result in a higher pressure than that in the SFA experiment. There is also a size effect for the two systems. This could be understood by looking at the force or pressure magnitudes in SFA experiments[2,7,8] and in the atomic force microscope (AFM).[41,67−69] In the SFA experiment, the very large contact area (the contact diameter varies from a few micrometers to a few hundred micrometers depending on the contact load) and the very compliant mica substrate will induce multidomain structures within the liquid film. The maximum repulsive pressure within the film could be around 150 atm or 15 MPa.[7] In biolubrication studies by the surface force balance, the highest pressure is reduced to 7.5 MPa.[22] However, in the AFM experiments,[41,67−69] the very rigid AFM tip and the nanometer contact area can easily make the repulsive pressure reach gigapascals. The present LVMD simulation is in fact dealing with the nanoscale contact between two rigid mica surfaces in an aqueous electrolyte. We find that the pressures corresponding to the repulsive forces shown in Figure 3 are roughly 1 order of magnitude higher than SFA measurements. The similar magnitude of pressure was also found by other grand canonical Monte Carlo simulation studies.[70] For this reason, direct force magnitude comparison between molecular simulation and SFA experiment is not feasible.

**B. Hydration Structure, Ionic Distribution, and Their Relations to the Hydration Force.** Figure 4 shows at a large distance of $D$ = 2.13 nm the density distributions of water molecules, the $K^+$ ions, and $Cl^-$ co-ions along the normal direction in the 1 M KCl electrolyte solution. The adsorbed peak of water near mica surface and its first and second hydration peaks in the 1 M KCl solution are similar to the X-ray reflectivity experimental results for pure water near the mica surface,[39] as well as to those in previous molecular simulations.[33,34] Further studies show that the in-plane hydration structures of water in KCl electrolyte are similar to those in the previous work.[33] The adsorbed water molecules are in an ordered phase and are directly situated above the ditrigonal cavities of the mica surface, while the first hydration water molecules are in a more disordered liquid phase.

The ionic density distributions of $K^+$ ions and $Cl^-$ co-ions seem to play more important roles in the development of repulsive hydration forces between mica surfaces in KCl

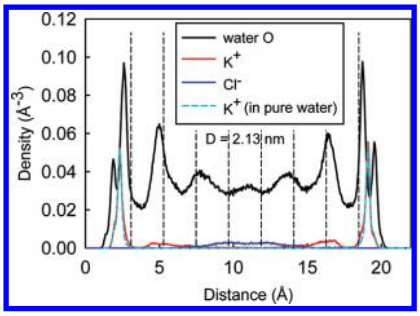


**Figure 4.** Water, $K^+$ ion, and $Cl^-$ co-ion density distributions along the normal direction in 1 M KCl electrolyte at $D$ = 2.13 nm thickness. $K^+$ ion density distribution in pure water droplet (dashed blue) is also shown in the figure for comparison. The perpendicular dashed lines represent different bins of water molecules for further diffusion analysis.

electrolyte. We first consider these distributions near mica surfaces. Figure 4 shows that the attached $K^+$ ions near mica surfaces are located between the adsorbed water peak and the first hydration peak, exhibiting exactly the same ionic distribution as those when mica is immersed in pure water (the dashed blue line). If we assume that the mean density of $K^+$ is 0.02 Å$^{-3}$ over the width of this peak, which is around 1.14 Å, then the cation density near the mica surface could be as high as $2.28 \times 10^{18}$ m$^{-2}$. Because mica has a very high surface charge density $\sigma = -2.1 \times 10^{18}$ e/m$^2$, the above calculation suggests that whether the mica sheet is in pure water or in 1 M KCl electrolyte solution, the mica surface charge density is always compensated by the nearest $K^+$ ions. The additional $K^+$ ions in the KCl electrolyte are largely situated in the diffuse layer away from the mica surfaces (see Figure 4). Note that the 0.02 Å$^{-3}$ mean density of $K^+$ ion near mica surface corresponds to an extremely high ionic concentration, which is about 33 M. This value is about 50% larger than the surface concentration of ions predicted by the theory.[1,71] Figure 4 also shows that most of the $Cl^-$ co-ions are located in the central diffuse layer between the two mica surfaces, consistent with the theoretical prediction for anions confined between negatively charged surfaces in electrolytes.[1]

Starting from $D$ = 1.99 nm ($n$ = 6) hydration film, Figure 5 shows the detailed water and ionic density distributions during the normal compression of the KCl electrolyte between mica surfaces. As the number of hydration layers decreases from 6 to 3 ($D$ is reduced from 1.99 nm to 0.99 nm in panels a−d), the $K^+$ ions and $Cl^-$ co-ions in the diffuse layer are gradually squeezed toward the midplane, accompanied by the significant increase in repulsive hydration force (see Figure 3). These are clearly seen from the snapshots of hydration structures shown in Figure 6. The fully hydrated ions and co-ions in the diffuse layer play a dominant role in building a "hydration bridge" between mica surfaces to support large external loads. Under the extreme confinement ($D$ = 0.75 nm, panel e), the $K^+$ ions in the diffuse layer are forced to adsorbed on mica surfaces, and only $Cl^-$ anions are left in the midplane. The direct contact of $K^+$ hydration shells on the two mica surfaces results in a repulsive hydration force as large as 16.5 nN (not shown in Figure 3) between mica surfaces. It should be noted that during the compression process, many $K^+$ ions and $Cl^-$ anions in the central diffuse layer are also squeezed out to the hydrophobic zone.


dx.doi.org/10.1021/la204603y | *Langmuir* 2012, 28, 5339−5349

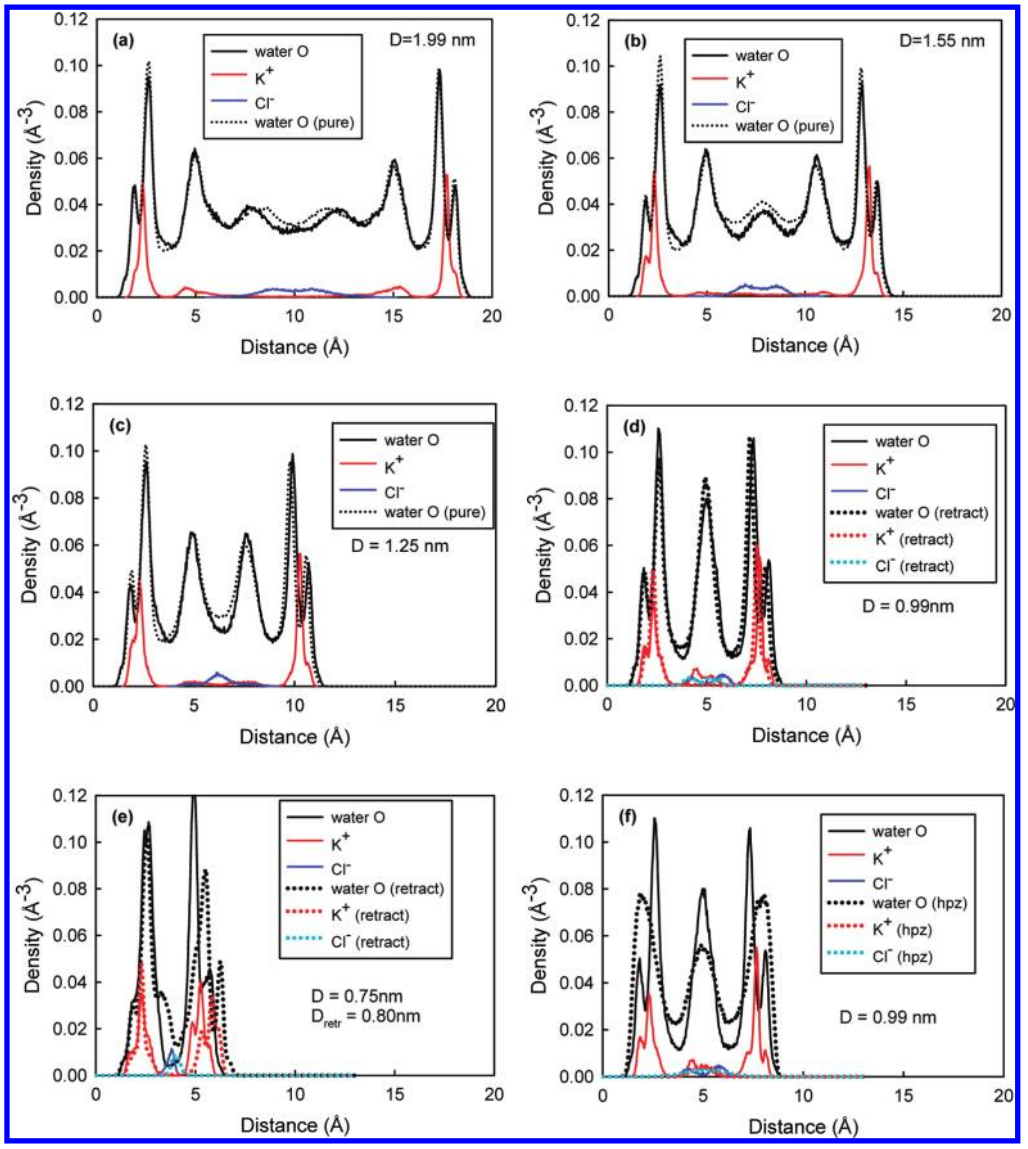


**Figure 5.** Water and ionic density distributions along the normal direction in 1 M KCl electrolyte films. In panels a–c, water density distributions in a pure water droplet between mica surfaces are also shown for comparison. In panels d and e, for which the film thicknesses $D$ = 0.99 and 0.75 nm, respectively, water and ionic density distributions during equilibrium retraction are also shown for comparisons. Panel f shows comparisons of water and ionic density distributions in mica pore and hydrophobic zone (hpz) in three hydration layers ($D$ = 0.99 nm).

For comparison, the first three panels in Figure 5 also show water density distribution when mica is immersed in pure water (the dotted line), which is slightly higher than those in KCl electrolyte due to the absence of hydrated $K^+$ and $Cl^-$ ions in the diffuse layer.

To understand the physical origin of the hydration force hysteresis upon retraction (Figure 3), in Figure 5 the equilibrium water and ionic density distributions during retraction at $D$ = 0.99 nm and $D$ = 0.8 nm are plotted in panels d and e. For the maximum hysteresis at $D$ = 0.8 nm, which corresponds to a slight repulsive force in Figure 3, panel e in Figure 5 shows that both $K^+$ and $Cl^-$ distributions undergo a slight outward shift. However, the increase in film thickness from $D$ = 0.75 to 0.8 nm does not lead to the formation of an additional hydration layer, resulting in a significant reduction in contact between the hydration shells associated with the adsorbed $K^+$ ions near mica surfaces. This is the origin of the maximum hysteresis occurring at $D$ = 0.8 nm. As the retraction process continues to proceed to $D$ = 0.99 nm, where the central hydration layer is developed (panel d in Figure 5), no adsorbed $K^+$ ions are found to desorb from mica surfaces, even after several nanoseconds of MD equilibrium runs. The fully hydrated $Cl^-$ co-ions in the central diffuse layer are able to provide repulsive hydration force, but with less magnitude as compared to the one during compression. Further studies show that as the mica surfaces are continuously being separated to form thicker hydration layers, some $K^+$ ions begin to desorb or release from mica surfaces to become diffusive ions. Consequently, force hysteresis gradually disappears at $D$ = 1.55 nm. The mechanism of the "forced adsorption" of diffusive $K^+$ ions under extreme confinement and the subsequent "slow desorption" of adsorbed $K^+$ ions during retraction explains the origin of the hydration force hysteresis.

The snapshots of the hydration structures during compression are shown in Figure 6. These molecular configurations clearly show that most of the $K^+$ ions are close to the negatively charged mica surfaces due to the ion–ion mutual repulsion,[1] and $Cl^-$ anions are situated in the central region. Note that in


dx.doi.org/10.1021/la204603y | Langmuir 2012, 28, 5339–5349

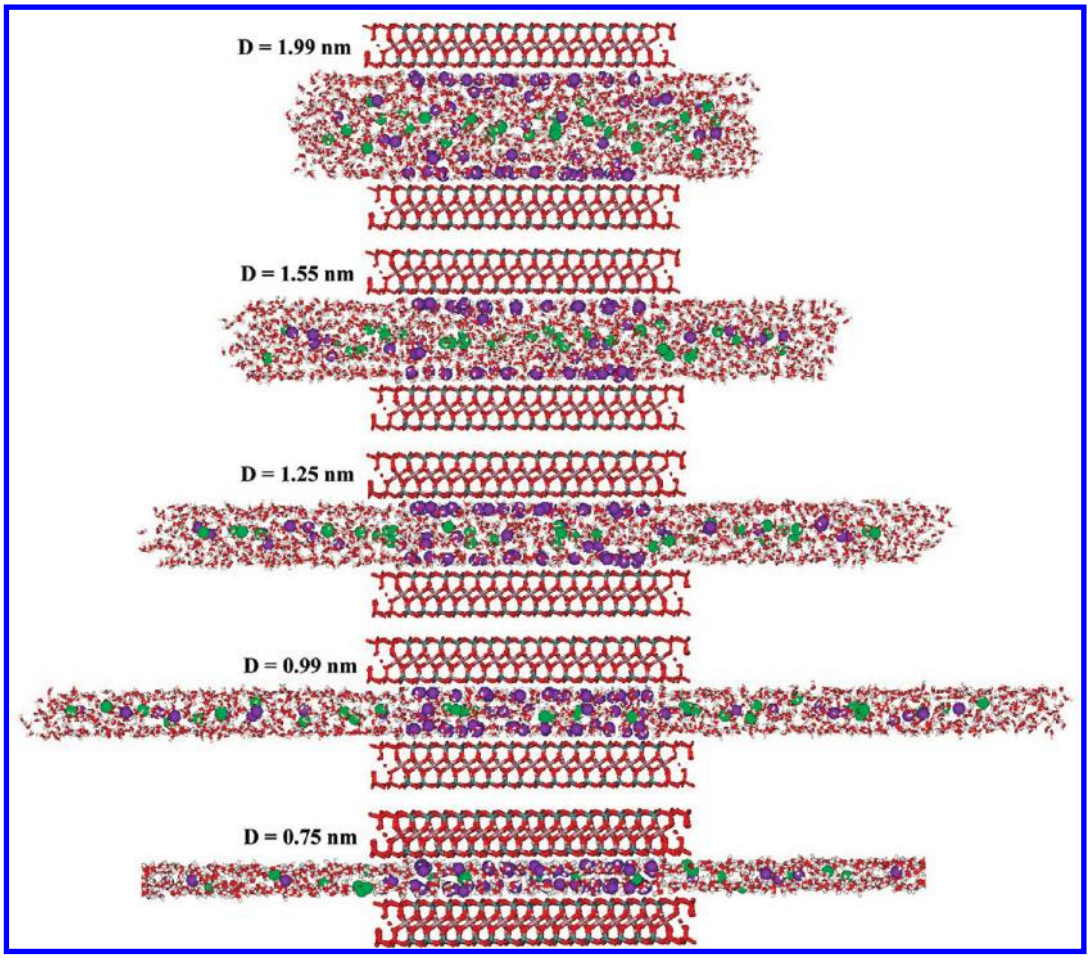


**Figure 6.** Snapshots of the different hydration structures of 1 M KCl electrolyte at $D$ = 1.99−0.75 nm thickness. The dark-pink and green spheres represent $K^+$ ions and $Cl^-$ co-ions, respectively.

the side hydrophobic pores, the squeezed out $K^+$ ions and $Cl^-$ co-ions are fully hydrated and are close to the midplane between two smooth hydrophobic walls. This is largely due to the very high hydration energies of the two species, making them difficult to directly contact hydrophobic surfaces. Comparisons of water and ionic density distributions in both mica and hydrophobic pores at $D$ = 0.99 nm distance are shown in panel f of Figure 5. The three hydration peaks in hydrophobic zone (hpz) are clearly seen. In particular, both fully hydrated $K^+$ ions and $Cl^-$ co-ions are located in the central region, corresponding to the $D$ = 0.99 nm snapshot in Figure 6.

**C. Diffusion of Different Species.** Given the strong repulsion between two mica surfaces in 1 M KCl electrolyte within ∼2 nm distance, we now consider the diffusion behaviors of water and ionic species in the confined electrolyte. The fluidity of water confined between two mica surfaces has been studied extensively in SFA experiments during the past two decades.[9,72−75] Studies by surface force balance showed that the fluidity of pure water is very similar to its bulk value when confined down to subnanometer films.[74,75] Previous molecular simulation work showed that the diffusion of water between mica surfaces under subnanometer confinement decreases by at most 2 orders of magnitude as compared to its bulk value.[23,33,34,47] It would be interesting to see how the hydrated metal ions and co-ions could influence the water diffusion behavior, and how these hydrated species themselves diffuse in confined aqueous electrolyte. For the confined geometry, the two-dimensional diffusion constant can be calculated from the Einstein relation:[76]

$$D_{xy} = \left\langle |r_{xy}(t) - r_{xy}(0)|^2 \right\rangle / 4t \tag{4}$$

where $r_{xy}(t)$ is the molecular position in the $x$−$y$ plane. In practice, to improve the statistical quality, the time average "⟨⟩" is computed on the basis of the particle number average and time origin average. The resulting mean-square displacement (MSD) of particles in the $x$−$y$ plane, defined as MSD = $\langle |r_{xy}(t) - r_{xy}(t_0)|^2 \rangle$, is usually quite smooth as shown in Figure 7.

Initially, the diffusion behaviors of water molecules in different cross sections parallel to mica surface are studied. To calculate these, the density distribution curve of water molecules is divided into nine bins (see Figure 4). The MSDs of water are then accumulated in each bin. If the particle positions at times $t$ and $t_0$ are in different bins, one-half of MSD will be contributed to each bin. For the diffusion calculations of $K^+$ ions and $Cl^-$ co-ions, the same procedure is performed but using different bin division. Part a in Figure 7 shows the variations of MSDs of water molecules versus time in different bins ($X$) in $D$ = 2.13 nm film. The diffusion constants in these bins are obtained by calculating the slopes of the MSD curves according to equation (4), as shown in part c of Figure 7. Obviously, the diffusion of water molecules reaches the maximum in the midplane and approaches the minimum close to the mica surface. The difference between the two could


dx.doi.org/10.1021/la204603y | Langmuir 2012, 28, 5339−5349

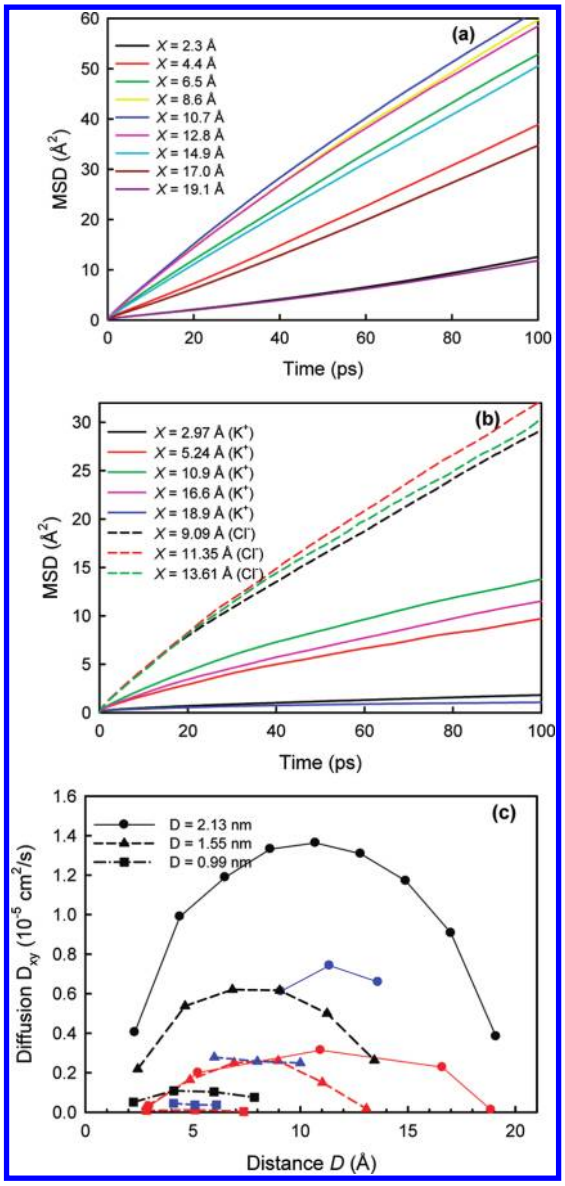


**Figure 7.** (a) The mean-square displacements (MSDs) of water molecules in different bins in $D$ = 2.13 nm KCl electrolyte film. (b) The MSDs of $K^+$ (solid lines) and $Cl^-$ (dashed lines) in different bins in the same $D$ = 2.13 nm electrolyte film. (c) The variations of diffusion constants versus bin position for water (black), $K^+$ (red), and $Cl^-$ (blue) species at three different film thicknesses.

be as large as 2.5 times of the minimum. The variations of the MSDs of $K^+$ ions and $Cl^-$ anions in $D$ = 2.13 nm film are shown in part b of Figure 7. It is seen that the overall diffusion of $Cl^-$ co-ions (the dashed lines in the figure) is higher than that of $K^+$ ions (the solid lines). In particular, the mobility of $K^+$ ions near mica surfaces is almost frozen. The distributions of diffusion constants for water molecules (black symbols), $K^+$ ions (red symbols), and $Cl^-$ anions (blue symbols) at three typical film thicknesses ($D$ = 0.99, 1.55, and 2.13 nm, respectively) are shown in part c of Figure 7. The figure shows that as the thickness of the aqueous electrolyte film decreases from 6 to 3 hydration layers, the diffusion constants of different species decrease by approximately 1 order of magnitude.

The variations of the averaged diffusion constants of water, $K^+$ ions, and $Cl^-$ co-ions versus the film thickness are shown in Figure 8. The figure also includes the results from the previous studies for pure water[47] and the TIP4P bulk water[77] (multiplied by a factor of 2/3 for the 2D diffusion) for comparisons. There are four conclusions drawn from Figure 8: (1) The overall diffusion of water molecules in 1 M KCl electrolyte film is slower than that in pure water droplet and is approximately within 3 orders of magnitude less than the bulk value of TIP4P water[77] under $D$ = 0.75 nm extreme confinement. (2) Diffusions of $K^+$ ions and $Cl^-$ co-ions in electrolyte are usually slower than water molecules. (3) $Cl^-$ anion initially has a faster diffusion than $K^+$ ion at larger distance, but soon becomes comparable to $K^+$ ion in the range of $D$ = 1−1.25 nm and much slower than $K^+$ ions under extreme confinement. This is the consequence of the severe deformation of $Cl^-$ hydration shells under subnanometer confinement (see section III.D) that reduces the mobility of $Cl^-$ co-ions. (4) The overall diffusion behaviors of the confined species (water, $K^+$, and $Cl^-$) at three hydration layers ($D$ = 0.99 nm) and above are quite fast and are within 2 orders of magnitude slower than the bulk water diffusion. At the same time, they have significant load bearing capacity as seen in Figure 3. These findings are consistent with recent experimental results of ionic transport in pressure solution in SFA measurement.[78]

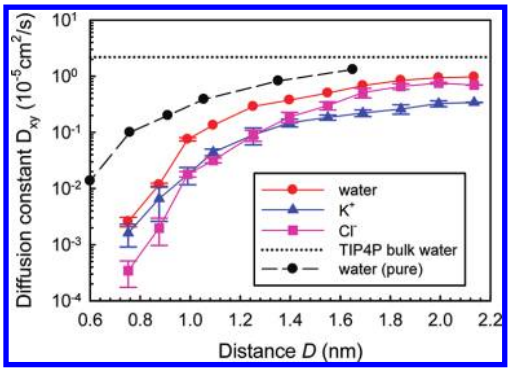


**Figure 8.** The variations of the averaged diffusion constants for different species in 1 M KCl electrolyte solution versus the mica gap distance. For comparison, diffusion constants in pure water droplet (black dot) in mica pore and in the TIP4P bulk water (dotted line) are also shown in the figure. Error bars indicate the variance. For water diffusion, error bars at larger distances are not shown because the variances at these distances are smaller than the symbols.

**D. Origin of the Load Bearing Capacity of Electrolyte under Confinement.** *Explanation from Continuum Double-Layer Repulsion Theory.* The strong repulsive hydration force between two mica surfaces in the 1 M KCl electrolyte within the last 2.0 nm gap is clearly associated with the role of $K^+$ ions and $Cl^-$ co-ions in the salt solution. The question is how do these two species in the solution make the electrolyte film so strong to support a very large repulsive load? To answer this question, we first consider the continuum electrostatic double-layer force between two mica surfaces in an electrolyte. From the thermodynamics definition of the pressure and the Poisson−Boltzmann equation, the pressure between two charged mica surfaces in an aqueous electrolyte can be calculated as:[1]

$$P(D) = kT(\rho_{\text{mid-total}}(D) - \rho_{\text{bulk-total}}) \quad (5)$$

in which $\rho$ is the sum of the total number density of ions and co-ions, $k$ is the Boltzmann constant, and $T$ is the temperature.


dx.doi.org/10.1021/la204603y | Langmuir 2012, 28, 5339−5349

Figure 5 shows that for $D$ = 0.75−1.99 nm electrolyte films, the averaged total ion density (including $K^+$ ions and $Cl^-$ anions)

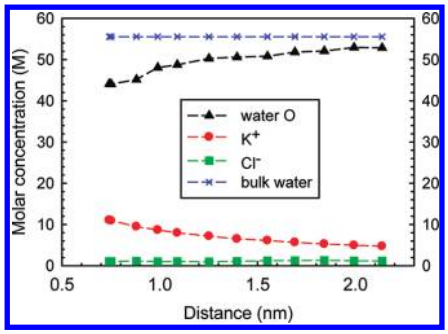


**Figure 9.** The variations of the molar concentrations versus mica gap distance for different species in 1 M KCl electrolyte film. For comparison, the molar concentration of bulk water is also shown in the figure.

in the midplane, $\rho_{midtotal}(D)$, varies from about 0.01 to 0.003 $Å^{-3}$ = (100−30) × $10^{26}$ $m^{-3}$. The total bulk density of ions in 1 M KCl electrolyte is $\rho_{bulk\text{-}total} = \rho_{K^+} + \rho_{Cl^-} = 2 \times 6.022 \times 10^{26}$ $m^{-3}$. Consequently, at $T$ = 298 K, the electrostatic double-layer pressure between the two mica surfaces at $D$ = 0.75−1.99 nm distances in the 1 M KCl electrolyte is around $P$ = 36−7 MPa. The characteristic length or the Debye length of the double-layer pressure in 1:1 KCl electrolyte is equal to $0.304/\sqrt{[KCl]}$ nm,[1] where [KCl] (=1.0) is the mole concentration of KCl electrolyte. This value is slightly larger than the decay length (0.28 nm) of the repulsive hydration force (see section III.A). Multiplying the double-layer pressure by the central mica area in the present simulation system ($A$ = 15 $nm^2$), the total repulsive force is in the range of 0.54−0.1 nN (see the double-layer force in Figure 3). This value is much less than the hydration force obtained in LVMD simulation, demonstrating that the short-range hydration force is much stronger than the continuum double-layer forces.[1]

*Explanation from the Pair Correlation Functions between Different Species.* From a mechanics point of view, the molar contents of different species in the confined electrolyte and the associated hydration structures should be ultimately responsible for the observed mechanical properties of KCl electrolyte film. Figure 9 shows the variations of the molar concentrations of different species in the mica pore versus the film thickness. It is interesting to see that water molar concentration is in fact decreasing as compared to its bulk value as the degree of confinement increases. In contrast, the concentration of $K^+$ ions is increasing due to the original counterions attached to the mica surfaces, while the concentration of $Cl^-$ co-ions remains almost constant around 1 M. This trend of variations in molar concentrations for different species implies that, perhaps, $K^+$ ions might play a major role in the load bearing capacity.

Because both $K^+$ ions and $Cl^-$ co-ions have very large hydration energies and approximately the same coordination number in the first hydration shell,[55,56] the interactions between different hydration shells of these two species should be closely related to the repulsive hydration force between mica surfaces. To further gain insights into these hydration shell interactions, in Figure 10 we plot the ion−water pair correlation functions g($r$) for $K^+$ and $Cl^-$. As shown in part a in Figure 10, the position of the first hydration peak of the $K^+$−water pair correlation function $g_{K-O}(r)$ has almost no change during the compression from $D$ = 1.99 nm to $D$ = 0.75 nm. The first hydration radii of the $K^+$ ions in different film thicknesses are located exactly at $r_{1-K}$ = 2.86 Å.[55] This phenomenon indicates that there is a very "hard" first hydration shell for $K^+$ ions. Furthermore, in the range of $D$ = 0.99 nm to $D$ = 1.99 nm, the first hydration peak is slightly higher than that of the $K^+$ ion in bulk water.[55] This slight increase in hydration peak under compression will lead to a slight increase in hydration number (not shown in the figure). Under $D$ = 1.99 to 0.99 nm confinements, the $g_{K-O}(r)$ is obtained only for the $K^+$ ions fully hydrated in the diffuse layer. Under the extreme confinement of $D$ = 0.75 nm, most of the $K^+$ ions are forced to adsorb on mica surfaces (see panel e in Figure 5) and become only partially hydrated. Under such circumstances, the $g_{K-O}(r)$ is calculated for all of the metal ions in the mica pore, and, consequently, its magnitude is reduced. However, the first hydration shell is still located at $r_{1-K}$ = 2.86 Å.

As compared to $g_{K-O}(r)$, the pair correlation function $g_{Cl-O}(r)$ is much "softer" (panel b in Figure 10). The first hydration shells under $D$ = 1.99 to 0.75 nm confinements undergo inward shifts relative to the bulk $g_{Cl-O}(r)$.[55] In particular, at $D$ = 0.75 nm thickness, this shift reaches a value of 0.2 Å away from the bulk hydration radius $r_{1-Cl}$ = 3.23 Å.[55] Note that because $Cl^-$ co-ions are fully hydrated in the diffuse layer, at large gap distances (e.g., $D$ = 1.99 nm), the $g_{Cl-O}(r)$ is already very close to the bulk $g_{Cl-O}(r)$.[55]

The more interesting finding is related to the second hydration shell of $K^+$ ions. Under $D$ = 1.99 to 1.25 nm confinements, the second hydration shell of $K^+$ ions still

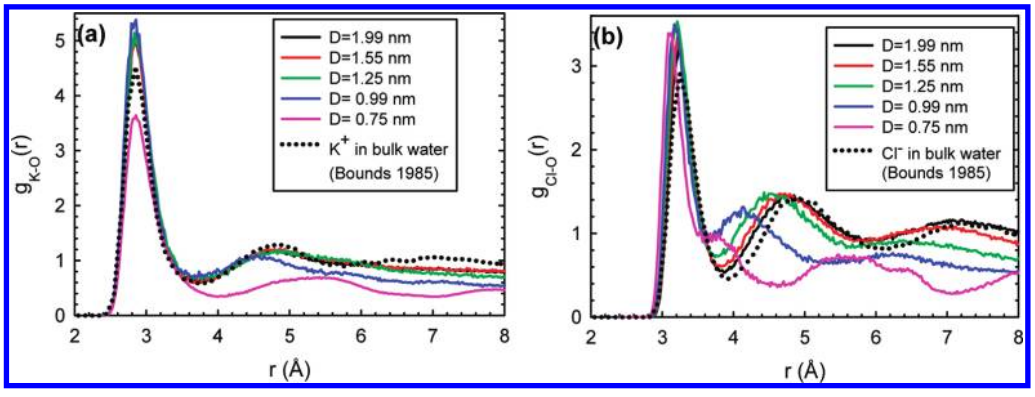


**Figure 10.** The variations of pair correlation functions of (a) $K^+$−water and (b) $Cl^-$−water in 1 M KCl electrolyte solution under different degrees of confinement.


dx.doi.org/10.1021/la204603y | Langmuir 2012, 28, 5339−5349

remains very rigid, because the second peak in $g_{K-O}(r)$ completely coincides with the bulk value at $r_{2-K}$ = 4.82 Å. It is only at the $D$ = 0.99 nm gap distance that an inward shift of 0.25 Å (or ∼5% of the second hydration radius) happens. Under the extreme confinement of $D$ = 0.75 nm, the second hydration shell of $K^+$ ions spreads out due to the depletion of water in electrolyte film. In contrast to $K^+$ ions, panel b in Figure 10 shows that when the film thickness is decreased from $D$ = 1.99 nm to $D$ = 0.75 nm, the second hydration shell of $Cl^-$ co-ions shrinks by ∼1 Å, or by ∼21% relative to $r_{2-Cl}$ = 4.85 Å. This significant difference in rigidity between the $g_{K-O}(r)$ and $g_{Cl-O}(r)$ pair correlation functions strongly suggests that while both $K^+$ and $Cl^-$ species have the load bearing capability, the $K^+$ hydration shell is much stronger than the $Cl^-$ hydration shell.

One question concerns whether the ion-pair interactions, such as the K−K, Cl−Cl, or K−Cl pairs, contribute to the repulsive hydration force. Because the free energies of hydration for $K^+$ and $Cl^-$ are much larger than the ion-pair interaction energies, these ions and co-ions are well dispersed in aqueous electrolyte (see Figure 6 for the molecular configurations). Further calculations for the ion−ion pair correlation functions for the K−K, Cl−Cl, and K−Cl pairs show that the first correlation peak in $g_{K-K}(r)$ under different confinements is well above 5.3 Å and essentially has no change with the degree of confinement, while $g_{K-Cl}(r)$ and $g_{Cl-Cl}(r)$ exhibit significant deformations as the degree of confinement increases. These results indicate that $K^+$ ions are well separated by the water molecules in the first hydration shells and the K−K ion-pair interaction is mainly determined by their first hydration shell interactions. On the other hand, the Cl−Cl and K−Cl ion-pair interactions are mediated by their first hydration shell interactions. These two ion-pair interactions show a very soft behavior as compared to the hydration shell interactions of $K^+$ ions. Therefore, we conclude that the load bearing capacity of the dense KCl electrolyte under nanometers confinement is largely attributed to the critical role of the hydrated $K^+$ ion, which has a tenacious hard hydration shell. The concurrent fluidic behavior of water molecules in this hydration shell, as evidenced by the significant diffusion even under extreme confinement, would suggest that even the simplest KCl electrolyte between charged mica surfaces is still a fairly good aqueous lubricant.[8]

## IV. SUMMARY AND CONCLUSIONS

Hydration force between molecularly smooth mica surfaces in electrolyte was investigated over 30 years ago.[2,3] While the model system was well-defined and fairly simple as compared to the more complicated aqueous systems at biological interfaces,[14,15,22] the mechanism of hydration force still needs to be understood. The present molecular simulation work, through the LVMD simulation method, directly simulates the force measurement procedure in the SFA experiment. While the fundamental difference in contact mechanics between the LVMD molecular simulation and surface force experiment is understandable, the repulsive force mechanism in dense KCl electrolyte should have a common ground. Simulation results show that during normal compression, the repulsive force in 1 M KCl electrolyte has a step-like oscillatory feature at $D$ > 1.0 nm distance, similar to the early experimental results by Pashley and Israelachvili.[5,7] The same force oscillatory behavior during retraction is also observed in simulations, but with much less hysteresis as compared to simple nonpolar fluids[48,51] at larger distances. This is largely due to the gradual release of adsorbed $K^+$ ions into electrolyte solution upon separation that provide strong repulsive forces between mica surfaces. We find that the continuum double-layer repulsion theory[1] could not explain this repulsive hydration force. From the detailed analysis of the ion−water pair correlation functions $g_{K-O}(r)$ and $g_{Cl-O}(r)$ under different degrees of confinement, we discovered that $K^+$ metal ion has a very hard hydration shell, while the hydration shell of $Cl^-$ co-ion is relatively soft. The former is mainly responsible for the load bearing capability of the confined KCl aqueous electrolyte.

Calculations of the hydration structures and ionic concentrations under different confinements show that $Cl^-$ anions are concentrated in the central diffuse layer, while a large portion of $K^+$ ions are attached to the negatively charged mica surfaces, where the concentration could be as high as 33 M. The diffusive behaviors of these two species are quite significant, but overall they are slower than that of water molecules. We find that the fluidity of water molecules in dense KCl electrolyte is retarded by the hydrated metal ions and co-ions, but is still significant in the sense that the diffusion constants of these water molecules under different degrees of confinement are reduced by at most 3 orders of magnitude as compared to its bulk value.

It should be noted that the present study only focuses on the KCl electrolyte solution. Recent surface force balance measurement found no evidence of repulsive hydration force between mica surfaces in aqueous $Cs^+$ solution.[79] Molecular dynamics simulations also showed that different alkali metal ions ($Li^+$, $Na^+$, $K^+$, and $Cs^+$) aqueous solutions exhibit very different friction behaviors.[37] Indeed, in our early simulation work,[80] preliminary results showed that the hydration repulsion in 1 M CsCl electrolyte is much weaker than those in KCl electrolyte. We attributed this difference in CsCl electrolyte to the very puffy and loose hydration shell of $Cs^+$ ion, and its relatively low hydration energy as compared to other alkali metal ions.[56] A thorough investigation on the hydration mechanisms of different alkali metal ions in electrolyte solutions will be beneficial to our complete understanding of the friction and lubrication behaviors of different aqueous electrolytes under confinement.

## AUTHOR INFORMATION

### Corresponding Author

*E-mail: leng@gwu.edu.

### Notes

The authors declare no competing financial interest.

## ACKNOWLEDGMENTS

This work was supported by the National Science Foundation (NSF 0904287), the American Chemical Society Petroleum Research Fund (PRF# 49596-DNI 5), and the National Energy Research Scientific Computing Center. I thank Yuan Xiang for his help in providing the pair correlation functions of $K^+$ ion and $Cl^-$ co-ion in bulk water.

## REFERENCES

(1) Israelachvili, J. N. *Intermolecular and Surface Forces*, 2nd ed.; Academic Press: New York, 1991.
(2) Israelachvili, J. N.; Adams, G. E. *J. Chem. Soc., Faraday Trans. 1* **1978**, *74*, 975.
(3) Pashley, R. M. *J. Colloid Interface Sci.* **1981**, *80*, 153.
(4) Pashley, R. M. *J. Colloid Interface Sci.* **1981**, *83*, 531.
(5) Israelachvili, J. N.; Pashley, R. M. *Nature* **1983**, *306*, 249.

(6) Pashley, R. M.; Israelachvili, J. N. *J. Colloid Interface Sci.* **1984**, *97*, 446.
(7) Pashley, R. M.; Israelachvili, J. N. *J. Colloid Interface Sci.* **1984**, *101*, 511.
(8) Raviv, U.; Klein, J. *Science* **2002**, *297*, 1540.
(9) Chai, L.; Goldberg, R.; Kampft, N.; Klein, J. *Langmuir* **2008**, *24*, 1570.
(10) Horn, R. G.; Smith, D. T.; Haller, W. *Chem. Phys. Lett.* **1989**, *162*, 404.
(11) Valle-Delgado, J. J.; Molina-Bolivar, J. A.; Galisteo-Gonzalez, F.; Galvez-Ruiz, M. J.; Feiler, A.; Rutland, M. W. *J. Chem. Phys.* **2005**, *123*, 034708.
(12) Grabbe, A.; Horn, R. G. *J. Colloid Interface Sci.* **1993**, *157*, 375.
(13) Perkin, S.; Goldberg, R.; Chai, L.; Kampf, N.; Klein, J. *Faraday Discuss.* **2009**, *141*, 399.
(14) Israelachvili, J.; Wennerstrom, H. *Nature* **1996**, *379*, 219.
(15) Leikin, S.; Parsegian, V. A.; Rau, D. C.; Rand, R. P. *Annu. Rev. Phys. Chem.* **1993**, *44*, 369.
(16) Ball, P. *Chem. Rev.* **2008**, *108*, 74.
(17) Skipper, N. T.; Lock, P. A.; Titiloye, J. O.; Swenson, J.; Mirza, Z. A.; Howells, W. S.; Fernandez-Alonso, F. *Chem. Geol.* **2006**, *230*, 182.
(18) Rotenberg, B.; Marry, V.; Vuilleumier, R.; Malikova, N.; Simon, C.; Turq, P. *Geochim. Cosmochim. Acta* **2007**, *71*, 5089.
(19) Fenter, P.; Sturchio, N. C. *Prog. Surf. Sci.* **2004**, *77*, 171.
(20) Klein, J. *Proc. Inst. Mech. Eng., Part J* **2006**, *220*, 691.
(21) Raviv, U.; Giasson, S.; Kampf, N.; Gohy, J. F.; Jerome, R.; Klein, J. *Nature* **2003**, *425*, 163.
(22) Chen, M.; Briscoe, W. H.; Armes, S. P.; Klein, J. *Science* **2009**, *323*, 1698.
(23) Leng, Y. S.; Cummings, P. T. *Phys. Rev. Lett.* **2005**, *94*, 26101.
(24) Braun, O. M.; Naumovets, A. G. *Surf. Sci. Rep.* **2006**, *60*, 79.
(25) Giovambattista, N.; Debenedetti, P. G.; Rossky, P. J. *J. Phys. Chem. C* **2007**, *111*, 1323.
(26) Giovambattista, N.; Rossky, P. J.; Debenedetti, P. G. *J. Phys. Chem. B* **2009**, *113*, 13723.
(27) Argyris, D.; Cole, D. R.; Striolo, A. *Acs Nano* **2010**, *4*, 2035.
(28) Shao, Q.; Zhou, J.; Lu, L. H.; Lu, X. H.; Zhu, Y. D.; Jiang, S. Y. *Nano Lett.* **2009**, *9*, 989.
(29) Shao, Q.; Huang, L. L.; Zhou, J.; Lu, L. H.; Zhang, L. Z.; Lu, X. H.; Jiang, S. Y.; Gubbins, K. E.; Shen, W. F. *Phys. Chem. Chem. Phys.* **2008**, *10*, 1896.
(30) Odelius, M.; Bernasconi, M.; Parrinello, M. *Phys. Rev. Lett.* **1997**, *78*, 2855.
(31) Boek, E. S.; Coveney, P. V.; Skipper, N. T. *J. Am. Chem. Soc.* **1995**, *117*, 12608.
(32) Park, S. H.; Sposito, G. *Phys. Rev. Lett.* **2002**, *89*, 085501.
(33) Leng, Y. S.; Cummings, P. T. *J. Chem. Phys.* **2006**, *124*, 074711.
(34) Leng, Y. S.; Cummings, P. T. *J. Chem. Phys.* **2006**, *125*, 104701.
(35) Meleshyn, A. *J. Phys. Chem. C* **2008**, *112*, 20018.
(36) Sakuma, H.; Kawamura, K. *Geochim. Cosmochim. Acta* **2009**, *73*, 4100.
(37) He, Y.; Shao, Q.; Chen, S. F.; Jiang, S. Y. *J. Phys. Chem. C* **2011**, *115*, 15525.
(38) Miranda, P. B.; Xu, L.; Shen, Y. R.; Salmeron, M. *Phys. Rev. Lett.* **1998**, *81*, 5876.
(39) Cheng, L.; Fenter, P.; Nagy, K. L.; Schlegel, M. L.; Sturchio, N. C. *Phys. Rev. Lett.* **2001**, *87*, 156103.
(40) Park, C.; Fenter, P. A.; Nagy, K. L.; Sturchio, N. C. *Phys. Rev. Lett.* **2006**, *97*, 016101.
(41) Fukuma, T.; Ueda, Y.; Yoshioka, S.; Asakawa, H. *Phys. Rev. Lett.* **2010**, *104*, 016101.
(42) Meleshyn, A. *J. Phys. Chem. C* **2008**, *112*, 14495.
(43) Derjaguin, B. V.; Landau, L. *Acta Physicochim. URSS* **1941**, *14*, 633.
(44) Verwey, E. J. W.; Overbeek, J. T. G. *Theory of the Stability of Lyophobic Colloids*; Elsevier: Amsterdam, 1948.
(45) Faraudo, J.; Bresme, F. *Phys. Rev. Lett.* **2005**, *94*, 077802.
(46) Cherepanov, D. A. *Phys. Rev. Lett.* **2004**, *93*, 266104.
(47) Leng, Y. S. *J. Phys.: Condens. Matter* **2008**, *20*, 354017.
(48) Lei, Y. J.; Leng, Y. S. *Phys. Rev. E* **2010**, *82*, 040501.
(49) Lei, Y. J.; Leng, Y. S. *Phys. Rev. Lett.* **2011**, *107*, 147801.
(50) Klein, J.; Kumacheva, E. *Science* **1995**, *269*, 816.
(51) Klein, J.; Kumacheva, E. *J. Chem. Phys.* **1998**, *108*, 6996.
(52) Xiang, Y.; Lei, Y. J.; Leng, Y. S., to be published.
(53) An alternative approach to make a uniform aqueous film in the entire region of mica and hydrophobic pores is to reduce the interaction strength between the hydrophobic wall and aqueous film while still keeping $\delta = 0$ Å (no backward shift of hydrophobic walls). After trial-and-error test, we find that reducing the 9-3 LJ surface potential by 2 orders of magnitude results in the same uniform aqueous film. At the same time, the calculated hydration force has no change at all.
(54) Jorgensen, W. L.; Chandrasekhar, J.; Madura, J. D.; Impey, R. W.; Klein, M. L. *J. Chem. Phys.* **1983**, *79*, 926.
(55) Bounds, D. G. *Mol. Phys.* **1985**, *54*, 1335.
(56) Jensen, K. P.; Jorgensen, W. L. *J. Chem. Theory Comput.* **2006**, *2*, 1499.
(57) Lee, S. H.; Rossky, P. J. *J. Chem. Phys.* **1994**, *100*, 3334.
(58) Israelachvili, J.; Pashley, R. *Nature* **1982**, *300*, 341.
(59) Miyamoto, S.; Kollman, P. A. *J. Comput. Chem.* **1992**, *13*, 952.
(60) Yeh, I. C.; Berkowitz, M. L. *J. Chem. Phys.* **1999**, *111*, 3155.
(61) Berendsen, H. J. C.; Postma, J. P. M; Vangunsteren, W. F.; Dinola, A.; Haak, J. R. *J. Chem. Phys.* **1984**, *81*, 3684.
(62) Leng, Y. S.; Lei, Y. J.; Cummings, P. T. *Modell. Simul. Mater. Sci. Eng.* **2010**, *18*, 034007.
(63) Fortes, M. A. *J. Colloid Interface Sci.* **1982**, *88*, 338.
(64) Cai, S. B.; Bhushan, B. *Philos. Trans. R. Soc., A* **2008**, *366*, 1627.
(65) Lei, Y. J.; Leng, Y. S. *Langmuir* **2012**, *28*, 3152.
(66) Johnson, K. L. *Contact Mechanics*; Cambridge University Press: New York, 1985.
(67) Li, T. D.; Gao, J. P.; Szoszkiewicz, R.; Landman, U.; Riedo, E. *Phys. Rev. B* **2007**, *75*, 115415.
(68) Khan, S. H.; Matei, G.; Patil, S.; Hoffmann, P. M. *Phys. Rev. Lett.* **2010**, *105*, 106101.
(69) Watkins, M.; Shluger, A. L. *Phys. Rev. Lett.* **2010**, *105*, 196101.
(70) Tambach, T. J.; Bolhuis, P. G.; Hensen, E. J. M.; Smit, B. *Langmuir* **2006**, *22*, 1223.
(71) Consider 1 M KCl electrolyte near a single mica surface. The ionic molar concentration near mica surface, according to the surface concentration equation of ions,[1] depends only on the surface charge density $\sigma$ and the ionic concentrations in the bulk, that is, $[K^+]_{surf} + [Cl^-]_{surf} = \sigma^2/2\varepsilon\varepsilon_0 kT + [K^+]_{bulk} + [Cl^-]_{bulk}$, where $\varepsilon$ is water dielectric constant ($\varepsilon = 80$) and $\varepsilon_0$ the vacuum permittivity, $k$ is the Boltzmann constant, and $T = 298$ K. For mica, $\sigma = -2.1 \times 10^{18}$ e/m$^2$ = 0.336 C/m$^2$. Given $[K^+]_{bulk} + [Cl^-]_{bulk} = 2$ M, we find that the surface concentration of ions $[K^+]_{surf} + [Cl^-]_{surf}$ is around 21.6 M. This value is about 50% less than the mean density of $K^+$ ions near mica surface obtained from MD simulation.
(72) Homola, A. M.; Israelachvili, J. N.; Gee, M. L.; McGuiggan, P. M. *J. Tribol.* **1989**, *111*, 675.
(73) Zhu, Y. X.; Granick, S. *Phys. Rev. Lett.* **2001**, *87*, 96104.
(74) Raviv, U.; Laurat, P.; Klein, J. *Nature* **2001**, *413*, 51.
(75) Raviv, U.; Perkin, S.; Laurat, P.; Klein, J. *Langmuir* **2004**, *20*, 5322.
(76) Allen, M. P.; Tildesley, D. J. *Computer Simulation of Liquids*; Clarendon Press: Oxford, 1987.
(77) Mahoney, M. W.; Jorgensen, W. L. *J. Chem. Phys.* **2001**, *114*, 363.
(78) Alcantar, N.; Israelachvili, J.; Boles, J. *Geochim. Cosmochim. Acta* **2003**, *67*, 1289.
(79) Goldberg, R.; Chai, L.; Perkin, S.; Kampf, N.; Klein, J. *Phys. Chem. Chem. Phys.* **2008**, *10*, 4939.
(80) Chow, P.; Leng, Y. S., unpublished work.